Coastal Florida Ecological Conservation

Assessing Recreational Fish Habitats in Florida using Earth Observations

Spring 2025 | California – Ames

April 4th, 2025

Authors: Audrey Chin (Analytical Mechanics Associates), Marco Conci (Analytical Mechanics Associates), Andrew Treptow (Analytical Mechanics Associates), Grace Markell (Analytical Mechanics Associates)

Abstract: The Atlantic tarpon (*Megalops atlanticus*) is a game fish species that is declining due to various environmental factors, including poor water quality, extreme temperatures, and habitat loss. The Bonefish & Tarpon Trust (BTT) is a non-profit that supports Atlantic tarpon conservation, often collaborating with the Florida Fish and Wildlife Conservation Commission - Fish and Wildlife Research Institute (FWC–FWRI) to inform restoration efforts and management plans. Over a 23-year period across the South Florida region we employed NASA Earth observations (EO) to investigate water quality parameters and habitats relevant to tarpon health for BTT and FWC-FWRI's conservation efforts. We mapped the extent of mangrove and seagrass habitats over the study period using the Landsat 5 Thematic Mapper (TM), Landsat 8 Operational Land Imager (OLI) and Landsat 9 OLI-2. We investigated turbidity and chlorophyll-*a* (chl-*a*) using Landsat observations, as well as the European Space Agency's (ESA) Ocean Colour Climate Change Initiative (OC-CCI) product. Sea surface temperature (SST) was investigated using the National Oceanic and Atmospheric Administration (NOAA)'s Multi-Scale Ultra High-Resolution SST Analysis (MUR SST) product. We conducted time-series analyses that showed changes in turbidity and chl-*a* in response to disturbance events, as well as increases in observed SST minimum and maximums by approximately 1°C over the study period. We created classification models for both habitats of interest, reporting a significant decline in mangrove habitat following Hurricane Irma and an increase in seagrass habitat during post-disturbance recovery periods. Both classification models faced limitations related to training data and resolution, impacting the accuracy of these results. Overall, we found that it was challenging to use EO to map seagrass habitat but feasible to identify changes in mangrove habitat and to evaluate water quality parameters over a large spatial and temporal scale.

Key Terms: Landsat, MODIS, mangrove, tarpon, seagrass, random forest, water quality, sea surface temperature

Advisors: Dr. Morgan Gilmour (NASA Ames Research Center), Dr. Juan Torres-Pérez (NASA Ames Research Center)

Lead: Lauren Webster (California – Ames)

1. Introduction

1.1 Background Information & Scientific Basis

The Atlantic tarpon (*Megalops atlanticus*) is a popular game fish species of major economic and ecological importance. In Florida, tarpon fishing is exclusively catch-and-release and contributes significantly to local economies by attracting recreational anglers to flats fisheries (Adams & Murchie, 2015). Tarpon fishing makes an estimated annual economic impact of $108 million on the Caloosahatchee River and Charlotte Harbor regions (Fedler, 2011) and drives over $100 million in retail sales within the Florida Everglades (Fedler, 2009). While no formal stock assessments have been made, trends in Central and South American commercial landings and U.S. recreational fishery data indicate that tarpon populations are declining due to habitat loss and degradation, poor water quality, overfishing, changes in freshwater flows, and extreme temperatures (Adams et al., 2014). These declines have motivated efforts to list tarpon as Vulnerable on the International Union for Conservation of Nature (IUCN) Red List (Adams et al., 2014). Tarpon conservation presents a strategic approach that not only supports a charismatic, economically important game fish species, but also benefits numerous other species that inhabit mangrove and seagrass habitats (Adams & Murchie, 2015).

Juvenile tarpon rely on mangrove forests for foraging and protection from predators, before moving to seagrass flats for foraging as sub-adults (Adams & Cooke, 2015). As habitat and species health are closely linked, identifying changes in these habitats provides relevant context for tarpon conservation. Although inland mangrove coverage within the Everglades has increased over the last three decades, outer coastal mangrove habitat has declined (Han et al., 2018). Coastal mangroves are especially vulnerable to large storm events, as demonstrated by significant mangrove loss following Hurricane Andrew (Han et al., 2018) and Hurricane Irma (Lagomasino et al., 2021).

Mangroves provide critical ecosystem services, such as protecting against coastal erosion and storm surge (Han et al., 2018). Similarly, seagrass flats also provide protection from storm disturbances by stabilizing sediments (Browder et al., 2013). Both mangrove forests and seagrass flats contribute to the biochemical processes that maintain water quality within each respective habitat (Browder et al., 2013). Water quality in turn influences seagrass and mangrove growth. Healthy mangrove and seagrass habitats benefit both tarpon and humans and the first step in protecting these ecosystems is broad spatial and temporal scale monitoring. This study assesses the feasibility of utilizing remote sensing data for such monitoring purposes.

NASA Earth observations can be applied to assess water quality parameters, including chlorophyll-*a* (chl-*a*), turbidity, and sea surface temperature (SST), using satellites such as Landsat (Ha et al., 2017) and MODIS (Carlson et al., 2018). Chl-*a* is a pigment found in all eukaryotic organisms that perform photosynthesis, and high concentrations of chl-*a* indicate high primary productivity. Turbidity is a measure of water clarity, affected by total suspended particulate matter. Coastal waters typically experience higher turbidity, which marine life is adapted to; however, unusually high turbidity can negatively impact aquatic life, for example reducing the amount of light available for seagrass photosynthesis (Samper-Villarreal et al., 2016). SST is a measure of the temperature on the surface of the ocean, which is relevant for tarpon health and seagrass growth. These water quality parameters are used globally to assess the health of marine ecosystems. MODIS is one of the longest continuously running SST remote sensing time series and shows a high level of accuracy when validated against in situ measurements (Espinoza-Morriberón et al., 2024). When compiled with other remote sensing products it can yield high spatial and temporal resolution. Researchers have achieved positive results calculating turbidity and chl-*a* levels using Landsat data (Dogliotti et al., 2015; Ha et al., 2017).

Remote sensing also provides valuable tools for evaluating habitat extent for ecosystems such as mangrove forests (Rhyma et al., 2016; Han et al., 2018) and seagrass beds (Topouzelis et al., 2018). Landsat sensors commonly used to map mangrove forests include Landsat 5 Thematic Mapper (TM), Landsat 7 Enhanced Thematic Mapper Plus (ETM+) and Landsat 8 Operational Land Imager (OLI; Han et al., 2018; Jamaluddin et al., 2022; Tran et al., 2022). Landsat 7 ETM+ and Landsat8 OLI have also been used for seagrass mapping (Wabnitz et al., 2008; Topouzelis et al., 2018). This study utilizes Landsat 5 TM, Landsat 8 OLI, and Landsat

9 OLI-2 data to classify mangrove and seagrass habitat across our study area for key years of interest around disturbance events.

1.2 Project Partners & Objectives

We partnered with the Bonefish & Tarpon Trust (BTT) as well as the Florida Fish and Wildlife Conservation Commission (FWC). BTT is a nonprofit organization dedicated to science-based bonefish and tarpon conservation. FWC manages Florida's wildlife resources. The Fish and Wildlife Research Institute (FWRI), a division of FWC, is responsible for conducting research to inform management decisions, and is especially interested in how seagrass and mangroves recover from severe weather events. The team identified two major projective objectives. The first objective was to analyze spatial and temporal patterns in SST and water quality to provide BTT with ecologically relevant context for understanding trends in tarpon habitat, health, and movement. The second objective was to map seagrass and mangrove extent over a two-decade period spanning multiple hurricane events to support BTT's tarpon conservation efforts and improve FWRI's ability to monitor coastal habitat change and target restoration efforts.

1.3 Study Area & Period

The study area included the entire Southern region of the Everglades, the Upper and Lower Keys regions, and the surrounding coastal waters monitored by the FWC's Coastal Habitat Integrated Mapping and Monitoring Program (CHIIMP), which encompasses 19,883 km^2 (Figure 1). For water quality analysis, we further divided the study area into seven management areas, adopted from previous BTT tarpon surveying research (Lombardo et al., 2024). Approximately 32.1 km between the Lower Keys and Dry Tortugas were excluded from the analysis due to the region's lack of mangrove forest or seagrass flat habitats. Within the study area, we focused mainly on the coastal regions of the Everglades, Biscayne Bay, and Florida Bay. The study period covered over two decades from 2002–2024, allowing us to assess the habitat change and habitat recovery following numerous storm events. For water quality analysis, we selected a six-month temporal resolution to capture seasonal shifts between the wet (June – October) and dry (November – May) seasons in South Florida.

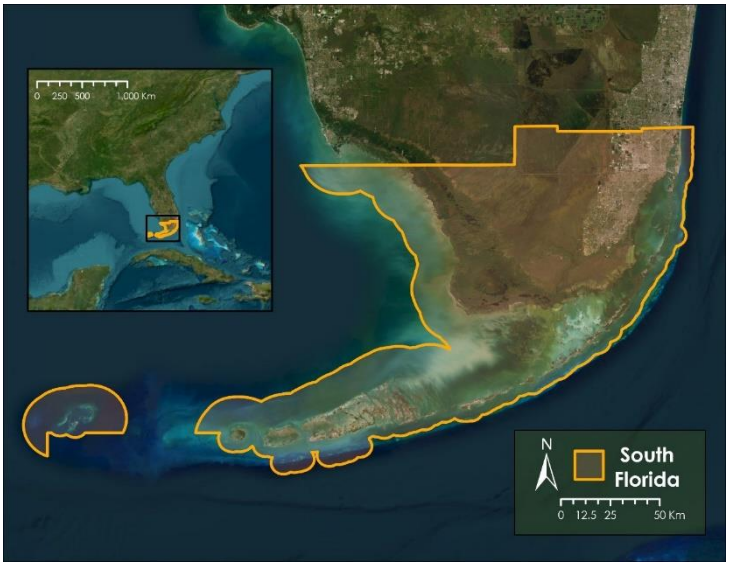

Figure 1. Map showing South Florida study area.

2. Methodology

2.1 Data Acquisition

2.1.1 Water Quality Data Acquisition

We took multiple approaches to analyzing water quality, using data with different data processing levels. Our assessment of water quality focused on two parameters – turbidity and chl-*a* levels. To analyze these parameters using Level-2 data, we used archived data from NASA's Landsat satellite series. We wrote a

Python (version 3.12.0) script that used the Microsoft Planetary Computer PySTAC Application Programming Interface (API) to retrieve Collection 2 Level-2 data from Landsat 5 TM, Landsat, 7 ETM+, Landsat 8 OLI, and Landsat 9 OLI-2 data (Table 1). For each of the seven management areas within our study area, we retrieved the median values for red, green, and blue remote sensing reflectance for all available dates across the 23-year period.

The water quality Level-4 data acquisition included three parameters – SST, chl-*a,* and the downwelling attenuation coefficient at 490 nm (Kd_{490}). We sourced these data from different data access protocols (DAP)s. The SST data were collected by NASA's JPL and compiled into one source by NOAA's Emergency Research Division. The chl-*a* and Kd_{490} data were collected from various government agencies across the world (ESA, NASA, NOAA, Japan Aerospace Exploration Agency [JAXA], and European Organization for the Exploitation of Meteorological Satellites [EUMETSAT]) as well as processed and compiled by ESA's Ocean Colour Climate Change Initiative (OC-CCI). For each parameter we used monthly averages of composited data.

We leveraged SST data, in °C, from NOAA's Multi-Scale Ultra High-Resolution (MUR) SST dataset. MUR SST aims to create a Level-4, bias corrected, 0.01 degree grid resolution, interpolated product that reports skin and subskin ocean temperatures. The satellites and sensors in this product include: Aqua MODIS, Terra MODIS, the Defense Meteorological Satellite Program (DMSP) Special Sensor Microwave Imagers (SSM/I), National Oceanic and Atmospheric Administration's (NOAA) Polar Operational Environmental Satellites (POES) Advanced Very High Resolution Radiometers (AVHRR), Aqua's Advanced Microwave Scanning Radiometer-EOS (AMSR-E), the Suomi National Polar-orbiting Partnership's (Suomi NPP) Visible Infrared Imaging Radiometer Suite (VIIRS), and several other in situ measurements from ships and buoys.

We sourced chl-*a* and Kd_{490} data from OC-CCI's ocean color (OC) product version 6, which aims to produce and validate the most comprehensive time-series from multiple sensors. The satellites and sensors used in this product include Aqua MODIS, ESA Envisat's Medium Resolution Imaging Spectrometer (MERIS), Sentinel-3's Ocean and Land Colour Instrument (OLCI), OrbView-2's Sea-viewing Wide Field of View Sensor (SeaWiFS), and Suomi NPP's VIIRS.

Chl-*a* concentration data in mg/m^3 were downloaded as monthly composites, generated by ESA's OC-CCI using a combination of OCI, OCI2, OC2, and OC_x algorithms depending on the water class, distinct bio-optical and biogeochemical properties of the water body. Kd_{490} data in units of m^{-1} were also downloaded as monthly composites from OC-CCI, which calculates Kd_{490} values using an algorithm from Lee (2005). Kd_{490} can be used to calculate the euphotic zone depth, the depth to which 1% of the photosynthetically available radiation reaches, which was used as a proxy for turbidity. Due to different sources and processing steps, the SST product had a ~1km spatial resolution and the chl-*a* and Kd_{490} product had ~4km resolution.

2.1.2 Habitat Mapping Data Acquisition

We downloaded Collection 2 Level-2 Landsat 5 TM, Landsat 8 OLI, and Landsat 9 OLI-2 data via Earth Explorer (Table 1). To acquire sufficient low cloud imagery while avoiding hurricane season, we narrowed our time range to the first six months of each year of interest (2006, 2010, 2015, 2018, 2019, 2024) then selected four images with <25% cloud cover for each of the four tiles required to fully encompass our study area.

Table 1. *Details from accessed remote sensing datasets.*

Earth Observation Dataset	***Date Range***	***Parameters***	***Acquisition Platform***
Landsat 5 TM, Collection 2 Level-2	2002 – 2013	blue, green, red, NIR, SWIR1, SWIR2, qa_pixel	Earth Explorer
Landsat 8 OLI, Collection 2 Level-2	2013 – 2024	blue, green, red, NIR, SWIR1, SWIR2, qa_pixel	SpatioTemporal Asset Catalog; Earth Explorer
Landsat 9 OLI-2, Collection 2 Level-2	2021 – 2024	blue, green, red, NIR, SWIR1, SWIR2, qa_pixel	SpatioTemporal Asset Catalog; Earth Explorer
Multi-Scale Ultra High-Resolution SST Analysis	2002 – 2024	SST	NOAA PolarWatch ERDDAP
ESA OC-CCI	2002 – 2024	Chl –*a,* Kd_{490}	UniData THREDDS Server

To create training data for our mangrove classification model, we downloaded the Mangrove Habitat in Florida and Florida Shoreline (1 to 12,000 Scale) datasets from the FWC online GIS database (FWC, 2023a; FWC, 2023b). To create training data for our seagrass classification model, we downloaded the Seagrass Habitat in Florida dataset available from the FWC online GIS database (FWC, 2024).

2.2 Data Processing

2.2.1 Water Quality Data Processing

The United States Geological Survey (USGS) stores Landsat Level-2 products as scaled 16-bit integers. USGS adopts this practice to store its data volumes more effectively. To convert the integer-value data we downloaded through the PySTAC API into the correct float value representing actual surface reflectance. We applied the following equation (United State Geological Survey [USGS], n.d.):

$$SR=DN \cdot SF+AO \tag{1}$$

Equation 1 calculates surface reflectance (*SR*) from the stored digital number (*DN*), scale factor (*SF*), and additive offset (*AO).*

We assessed water turbidity by calculating the Normalized Difference Turbidity Index (NDTI; Equation 2). Lizcano-Sandoval et al. (2022) found NDTI to be a useful estimation of turbidity in Florida's inland and shallow coastal waters.

$$NDTI = \frac{red - green}{red + green} \tag{2}$$

We used the Normalized Difference Chlorophyll Index (NDCI) to predict chl-*a* concentration (Equation 3). Mishra & Mishra (2012) proposed NDCI, finding that it performed better than traditional blue-green algorithms at discerning chl-*a* in environments that contain colored dissolved organic matter and other complex aquatic environments. We adopted the technique of Buma & Lee (2020) which calculates NDCI from NIR and red band values.

$$x=\frac{NIR-red}{NIR+red} \tag{3}$$

The Level-4 data used for water quality analysis was pre-processed into a uniform space-time grid, specifically corrected, and averaged into monthly composite values based on the location. Since the data were already spatially and temporally referenced with units assigned, we subset each variable into individual NetCDF files

for the entire study period. We clipped these NetCDF files to the individual tarpon management regions of interest using ArcGIS and saved them as new NetCDF files.

As a proxy for turbidity, we calculated the depth of the euphotic zone. We used Equation 4 (Zhao et al., 2013), to calculate the euphotic zone depth for the region of the Florida Keys.

$$Z_{eu} = 0.28 + \left(\frac{(395.92 \cdot 0.0092)}{(0.0092 + Kd_{490})}\right) \quad (4)$$

Equation 4 calculates the depth of the euphotic zone, Z_{eu} (m). It only requires Kd_{490} (m^{-1}) as a variable to input. Once we created and calculated the new variable, euphotic zone depth, we had all the necessary information to analyze the data.

2.2.2 Habitat Mapping Data Processing

We processed Landsat imagery in ArcGIS Pro (Version 3.3.0) to create multiband rasters by compositing the following six bands of interest: blue, green, red, near infrared (NIR), shortwave infrared (SWIR) 1, and SWIR2. Using the corresponding pixel quality assessment band, we removed clouds from each of the multiband rasters. We mosaicked the resultant cloud masked rasters together for each year of interest and clipped the result to our study area. This produced, for each year of interest, a cloud-free, six-band raster spanning our study area. These rasters provided the base imagery for both seagrass and mangrove mapping, although we conducted additional data processing steps for each of the habitat types.

For the mangrove-specific data processing, we selected three relevant indices to help distinguish mangroves from water and non-mangrove terrestrial areas. For each year of interest, we restricted surface reflectance values to the valid value range, then converted the data to floating point format using the appropriate scale factor and additive offset in Python (Version 3.10.16). Using these floating-point values, we calculated the Modified Normalized Difference Water Index (MNDWI; Equation 5; Xu, 2006), Normalized Difference Moisture Index (NDMI; Equation 6; Gao, 1996), and Normalized Difference Vegetation Index (NDVI; Equation 7; Rouse, 1973).

$$\text{MNDWI} = \frac{\text{green - SWIR1}}{\text{green + SWIR1}} \quad (5)$$

$$\text{NDMI} = \frac{\text{NIR - SWIR1}}{\text{NIR + SWIR1}} \quad (6)$$

$$\text{NDVI} = \frac{\text{NIR - red}}{\text{NIR + red}} \quad (7)$$

MNDWI was selected to help distinguish open water features while limiting error from built-up areas (Xu, 2006) along Florida's southeastern coastline and in the Florida Keys. NDMI is an index designed to approximate vegetation water content (Gao, 1996) and was included due to its strong performance at detecting changes in mangroves following disturbance events (Zhang et al., 2016). The NDMI formula shown above in Equation 6 was originally proposed by Gao (1996) under the name Normalized Difference Water Index (NDWI), but we have chosen to call it NDMI following Wilson & Sader (2002) and Zhang et al. (2016) to avoid confusion with the more commonly known NDWI index proposed by McFeeters (1996). NDVI is one of the most frequently used indices in mangrove mapping studies (Tran et al., 2022) and was included to identify vegetation.

To reduce misclassification of mangroves in inland areas, we used the Florida coastline shapefile (FWC, 2023b) to create a raster of distance to coastline from land (hereafter 'distance to coastline'), where each pixel within the interior of the coastline polygons was assigned a value equal to the Euclidean distance from the

center of the pixel to the nearest point on coastline and all other pixels were set to zero. We imported this raster into Python and appended it to the existing bands and indices to complete the ten-feature dataset.

We created our mangrove training data by converting the FWC coastline and mangrove shapefiles into rasters with 30m resolution in ArcGIS Pro. We chose to draw training data from two regions, selecting study area subsets in the Everglades and near Homestead, Florida, to represent both dense coastal mangroves and coastal mangroves that border agriculture and developed areas. We combined the coastline and mangrove rasters to create rasters classifying each pixel within the study area subsets as either non-mangrove terrestrial area (hereafter 'land'), water, or mangrove. We paired these habitat class rasters with processed Landsat imagery and calculated indices for corresponding spatial and temporal extents as well as the distance to coastline raster. This produced training data where each pixel was assigned a habitat classification as well as ten additional values corresponding to the six bands, three indices, and distance to coastline values.

For our seagrass-specific habitat mapping, one index was calculated to strengthen classification. Adapted from NDVI, Villa et al. (2013) introduced an index to identify aquatic vegetation, the Normalized Difference Aquatic Vegetation Index (NDAVI):

$$\text{NDAVI} = \frac{\text{NIR-blue}}{\text{NIR+blue}} \tag{8}$$

Equation 8 was added to the multi-band raster for each year. There is not a commonly agreed upon index for seagrass identification. We chose NDAVI over other indices due to its common use in larger study areas (Villa et al., 2014), as well as its lack of need for additional calculations (Liang et al., 2023; Li et al., 2023). Using the FWC coastline data, we removed land from each multiband raster for seagrass classification due to irrelevance in seagrass classification.

We created seagrass training data from the Florida Keys National Marine Sanctuary Seagrass Monitoring Project (Program 296), available through the Florida Statewide Ecosystem Assessment of Coastal and Aquatic Resources (SEACAR) Data Discovery. This point dataset reported in situ survey results across monitoring sites with percent cover values (average percentage of seagrass within ten 25 cm^2 quadrats along a 50 m transect line). For the year 2015, points that reported seagrass percent cover of at least 5% (0.5 Braun-Blanquet score) were classified as "Seagrass" for training data, with the rest of the monitoring sites being classified as "No Seagrass". This class designation follows the assumption that 30 m spatial resolution would not be able to differentiate between this threshold (Lizcano-Sandoval et al., 2022), as well as balancing the samples between each class.

2.3 Data Analysis

2.3.1 Water Quality Data Analysis

Using Python and the Matplotlib library (version 3.10.1), we created time series plots of turbidity and chl-*a* indices for each management area. We looked for cyclical trends in the time series, changes over time, differences between management areas, and impacts of known recorded severe weather events.

Using a Python script and the Matplotlib library, we created time series plots of estimated euphotic zone depth, chl-*a* concentrations, and SST for each management area. We calculated the mean monthly values of these variables over our study period. This is to demonstrate expected seasonal fluctuations, assess if they are changing annually, and observe the inherent variability of these water quality parameters. Using linear regressions, we calculated long-term trends among the minimum and maximum values seen in the monthly averages of the dry and wet seasons. Large environmental disturbance events were also included in our analysis of all variables to see if we could observe anomalous conditions after such events.

2.3.2 Habitat Mapping Data Analysis

We conducted the mangrove mapping data analysis in Python. To build the model, we randomly selected 50,000 pixels from the Everglades training data and 50,000 pixels from the Homestead training data to serve as samples. We randomly allocated 70% of these samples for model training and reserved the remaining 30% for model testing. Using the RandomForestClassifier function from the scikit-learn library, we constructed a random forest model. For the features, we used blue, green, red, NIR, SWIR1, SWIR2, MNDWI, NDMI, NDVI, and distance to coastline. For the model parameters, we selected 100 decision trees and set the class weight parameter to 'balanced' to adjust for unequal class frequencies in our training data.

To evaluate mangrove classification model performance, we ran the model on the testing dataset, constructed a confusion matrix, and calculated model accuracy, precision, and recall. We also calculated relative feature importance. To construct our mangrove maps, we applied the trained random forest model to the processed Landsat imagery for each year of interest. Finally, we calculated change in mangrove coverage from pre- to post- hurricane years and mapped these changes to better understand their spatial distribution.

We conducted the seagrass mapping data analysis in ArcGIS Pro using a pixel-based random forest model. We trained the classification model with the 2015 training data adapted from Program 296, and the 2015 Landsat multi-band raster with NDAVI calculated and land excluded. We chose 2015 for training due to more equivalence between classes in training data compared to other years. We selected 100 decision trees for this classification model and utilized all available training data for model training. Because of this, we tested accuracy using data from the FWC Seagrass Habitat in Florida dataset.

3. Results

3.1 Analysis of Results

3.1.1 Water Quality Time Series Analysis of Results

The study area waters were generally clear with overall low turbidity and chl-*a* levels. The calculated NDTI ranged from approximately -0.5 to 0.1 (positive NDTI values indicate higher turbidity and negative NDTI values indicate lower turbidity). The calculated NDCI values ranged from -0.4 to 0.5 (in optically clear water bodies NDCI is expected to hold values closer to – 1 with high algal biomass expected close to 1). Values near zero in both indices typically indicate low turbidity and chl-*a* concentrations. Some of the management areas showed noticeably higher NDTI and NDCI measurements than others. For example, Figure 2 shows the stratification of NDTI and NDCI levels between different management areas around the Florida Keys.

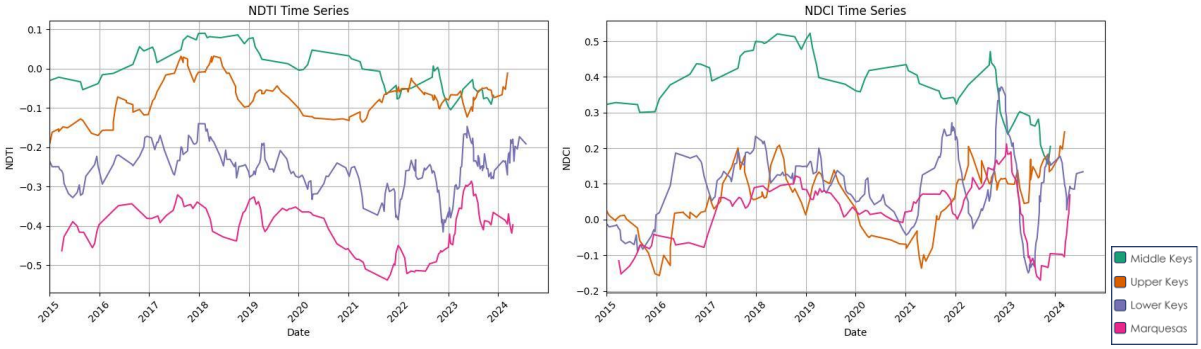

Figure 2. Median NDTI (left) and NDCI (right) for Selected Management Areas from 2015 – 2024.

We also plotted the index measurements, averaging month-by-month across all years. We observed that the NDTI and NDCI levels cycled on an annual basis. The Upper Keys were representative of most management areas, with highest NDTI and NDCI during the autumn and winter months (Figure 3).

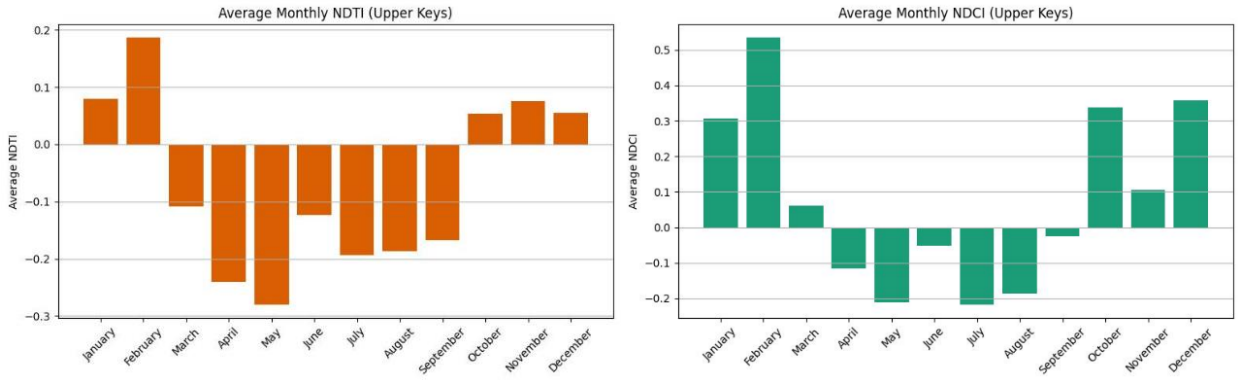

Figure 3. Average Monthly NDTI (left) and NDCI (right) for Upper Keys, aggregated across 2015 – 2024.

When using the different composites of satellite products for analyzing water quality, we saw varying results from the Landsat approach. Most notably is the analysis of SST, which was not easily analyzed with Landsat. Within our study area the minimum SST for averaged January values ranged from 17.5 to 25.7°C between 2002–2024. Six out of seven of the regions of interest showed an increase of minimum SST over this study period. Chokoloskee was the only region that showed a decreasing trend over the study period. Using simple linear regression of minimum SST versus time, the entire management region showed an average increase of 0.05°C per year ($R^2 = 0.31$).

We analyzed the maximum SST of averaged July values from each of the regions using simple linear regression. The maximum SST in July ranged from 29.3 to 32.3°C from 2002–2024 (Figure 4). The marine heat wave of 2023 coincided with the highest temperatures of any July during our 22-year study period. In all seven regions of interest, there was an increase in maximum SST during this period. This increase ranged from 0.045 – 0.056°C per year, averaging 0.05°C per year. For both minimum and maximum temperatures of the respective cold and warm seasons there is a similar trend of increasing extreme temperatures at a rate of over 1°C every 20 years.

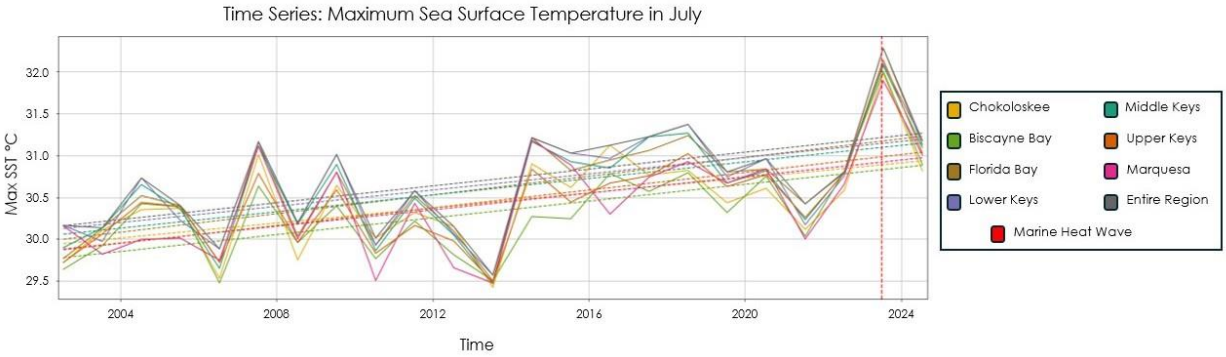

Figure 4. The maximum pixel value of SST from each management area during July, plotted from 2002 – 2024. The dashed trendlines are the same color as the solid lines, each representing one of seven management regions. The grey dashed line representing all the regions combined. Red vertical dashed line shows the 2023 Florida Keys marine heat wave.

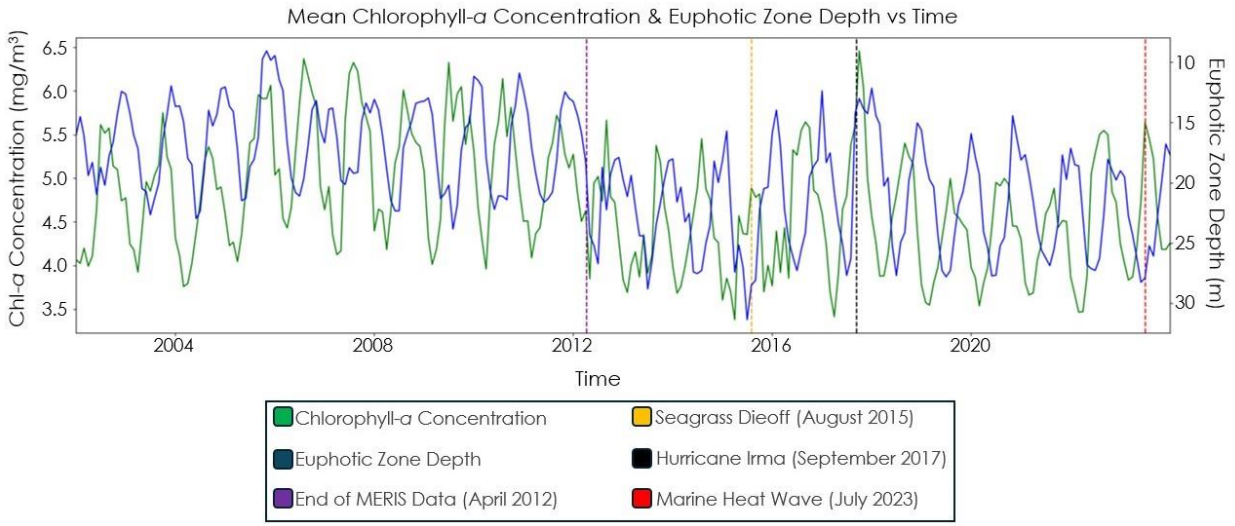

Figure 5. Chlorophyll-a (green) and the depth of the euphotic zone depth (blue) plotted monthly from 2002 – 2024. Significant events plotted as dashed vertical lines: The end of the MERIS mission (purple), a large seagrass die-off event (yellow), Hurricane Irma (black), 2015 Marine head wave (red).

Chl-*a* typically peaks around the fall while turbidity is typically highest in the winter. When averaged across the study region, chl-*a* ranged from 3.3–6.5 mg/m^3, and the euphotic zone depth ranged from 9–32 m. There is no obvious connection between the two parameters, although there appears to be a three-month lag time between their peak timings, with chl-*a* peaks occurring first. However, some disturbance events may indicate a relationship between these two parameters. First around August 2015 there was a seagrass die-off, at the same time there was anomalously low turbidity and chl-*a* values for the year. In contrast, Hurricane Irma coincided with extremely high turbidity and chl-*a* values. Finally, while the marine heat wave of July 2023 caused extremely high SST (Figure 4), it does not appear to lineup with any chl-*a* or turbidity anomalies. One important thing to note is that during 2012–2013 the values of chl-*a* and turbidity appear to decrease in terms of minimum and maximum for the majority of the rest of the study period.

3.1.2 Habitat Mapping Analysis of Results

The mangrove classification model yielded an overall accuracy of 95.24% when run on testing data from our training dataset. Model precision was 95.57% for land, 99.49% for water, and 85.70% for mangroves. Model recall was 96.73% for land, 99.28% for water, and 82.23% for mangroves. The feature with the highest relative importance was distance to coastline, followed by NDVI, NIR, and MNDWI (Table A1).

Computing pixel change between 2015 and 2018 model outputs showed large reductions in mangrove habitat along Florida's southeastern coast (Figure 6a). Computing pixel change between 2018 and 2019 model outputs showed moderate increases in mangrove habitat along Florida's southeastern coast (Figure 6b). For 2015, the model classified 1,455,308 pixels, or approximately 1,310 sq km, as mangroves (Figure A3). The model classified ~787 sq km as mangroves in 2018 (Figure A4) and ~1,094 sq km as mangroves 2019 (Figure A5). For the most recent year of interest, 2024, the model classified ~1,499 sq km as mangroves (Figure A6). For earlier years of interest, the model was likely less accurate due to differences in source imagery (see 3.2.2) and only classified ~196 sq km as mangroves for 2006 (Figure A1) and ~512 sq km as mangroves for 2010 (Figure A2).

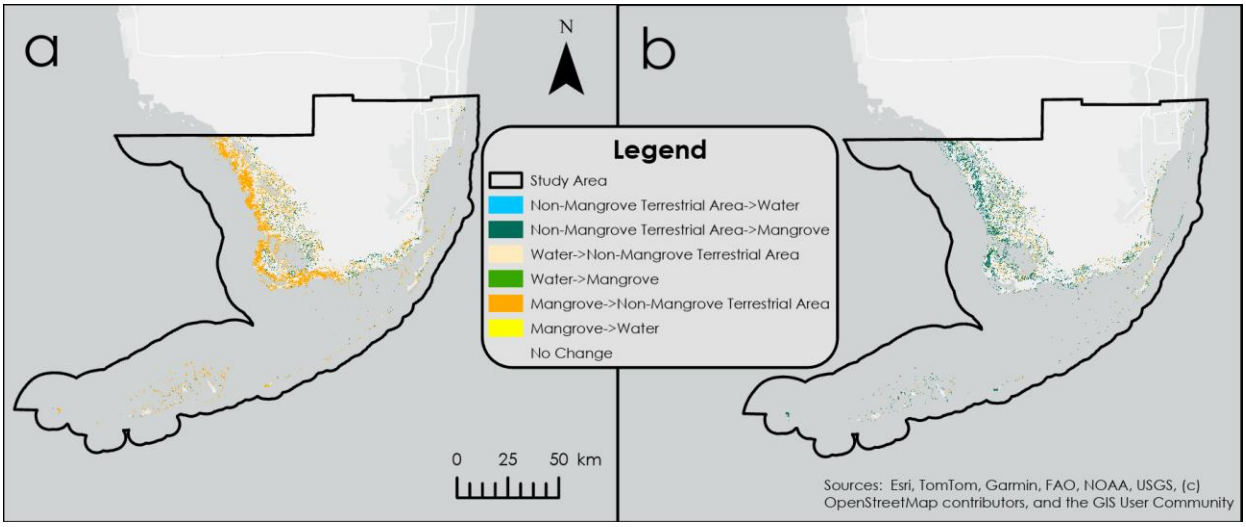

Figure 6. Mangrove change maps comparing classification model outputs from (a) 2015–2018 and (b) 2018–2019. Pixels classified differently in the two years compared are colored according to the appropriate class change. Pixels that did not change classifications between years being compared are transparent. Both maps share the same scale, orientation, and basemap credits.

The seagrass classification model yielded an overall accuracy of only 5% when ran on FWC testing data. A large source of error within the model was misclassification of seagrass habitat as a lack of seagrass. Due to prioritization of improving the low accuracy of the model, we did not conduct pixel change analysis between model outputs for seagrass habitats.

3.2 Errors & Uncertainties

3.2.1 Water Quality Errors & Uncertainties

Throughout this study, we used normalized difference indices such as NDCI, NDMI, NDTI, and NDVI, to analyze various factors relevant to the tarpon habit. These indices are sensitive to noise from the input variables and amplify any variance in the remote sensing surface reflection readings.

With regards to the use of composite products there are several errors and uncertainties. Unlike Landsat which has 30m spatial resolution, composite products result in the use of much coarser spatial resolution. This introduces a lot of uncertainty in the accuracy of the data, especially with near coastal areas. Coarse resolution can make it challenging to obtain representative data; for example, obtaining values within 1 km of land for SST and 4 km for chl-*a* and Kd_{490}. Another source of uncertainty is there also could be errors without bias correction from different sensors. We are not certain what caused the visible change in oscillation of both chl-*a* and euphotic zone depth, though a likely possibility is a change in the sensors incorporated into this composite product and without correction between sensors this shift is visible. Another layer of uncertainty is the processing of data from the sources before our acquisition of the data. When acquiring data from others there is a chance that the teams that compiled numerous data sources together could have introduced errors and uncertainties. Errors could stem from numerous sensors with different resolutions and recursion times being interpolated together. Not every study area will have an equal input from all sensors, and some may interpolate over land but not other sensors. Finally, due to the use of monthly composites, monthly values will not equally represent the whole month in some cases, for example if part of the month has no data due to clouds, the part of the month that does have data will be used to represent the entire month, even if conditions are different for these respective parts of the month.

3.2.2 Habitat Mapping Errors & Uncertainties

Both seagrass and mangrove mapping relied on cloud-masked, mosaicked rasters created from Landsat imagery. Cloud masking was imperfect, as the qa_pixel layer did not always align perfectly with clouds in the

Landsat imagery. Cloud masking also resulted in a small percentage (<5%) of our study area having NoData values for each year of interest, as some pixels were cloud masked for all of the images used to create a given year's composite.

Additionally, we trained both habitat classification models using 2015 imagery from Landsat 8 OLI, which has slightly different spectral bands than the earlier Landsat 5 TM. This difference could have contributed to lower accuracy in model outputs from earlier years (2006 and 2010) than later years with Landsat 8 OLI and Landsat 9 OLI-2 data. Another potential limitation of both habitat classification methodologies is the 30 m spatial resolution of Landsat surface reflectance data, limiting each model's ability to classify smaller patches of both mangrove islands and seagrass flats.

The mangrove training data did not include information about mangrove condition, so we were not able to train our model to distinguish damaged mangroves and healthy mangroves as two separate classes. Moreover, because the habitat class training data were primarily from 2014–2016, the majority of mangrove training data corresponded to healthy mangroves. As a result, our model likely overestimates mangrove "loss" following disturbance events as damaged mangroves could be classified as land. It is unclear what degree of mangrove damage results in this misclassification.

As previously mentioned, we designated a low threshold of at least 5% cover of seagrass constituting "seagrass" classification. This low threshold was necessary to have a relatively balanced training dataset between class values within the relatively small training data sample size (less than 500 pixels). This low threshold is not the most effective when determining the ecological health and function of a seagrass habitat, as it does not show change between higher seagrass densities. Furthermore, because the training data we created from Program 296 was small, all points had to be used to train the model and not used for accuracy testing. The FWC dataset used to test accuracy of the model contains polygons delineating "Patchy (Discontinuous) Seagrass" or "Continuous Seagrass", not including percent cover. Because percent cover within the Program 296 data were the main metric used to designate the threshold for seagrass classification within our classification model, this led to some incompatibilities with the training and testing data. Incongruencies between these datasets could have contributed to a misleading estimation of accuracy.

4. Conclusions

4.1 Interpretation of Results

4.1.1 Water Quality Interpretation of Results

SST extremes are increasing in both wet and dry seasons. This rate is on average 0.05°C per year. This trend agrees with other studies describing an increase of SST globally (Bulgin et al., 2020), though other reported trends are lower. While not always linked, significant disturbance events will affect chl-*a* and turbidity. The change in oscillation in 2012 of chl-*a* and turbidity was possibly caused by a miscalibration between sensors (Bindschadler, 2013) but could also be from larger temporal physical oscillations. The seagrass die-off event of 2015 occurred during low precipitation and dissolved oxygen period causing low chl-*a* and turbidity (Hall et al., 2016). Hurricane Irma resulted in intense mixing and less stratification, explaining the high chl-*a* and turbidity.

4.1.2 Habitat Mapping Interpretation of Results

The decrease in model-classified mangrove habitat from 2015 to 2018 is most likely the result of Hurricane Irma, which made landfall in southern Florida in September 2017. The subsequent increase in model-classified mangrove habitat from 2018–2019 likely reflects partial recovery of mangrove habitat following Hurricane Irma. The mangrove extent change maps, while not perfectly accurate, illustrate a general trend of mangrove damage and subsequent recovery following a major storm event. As some climate models predict increases in the intensity of Atlantic hurricanes over the 21st century (Doyle & Girod, 1997), understanding patterns of mangrove dieback and recovery in the wake of hurricanes is especially important for FWC to effectively steward Florida's mangroves and the fisheries they support.

Due to the lack of confidence in the results of the seagrass classification model, result interpretations cannot be appropriately supported. The model-classified seagrass extent was the lowest in 2006 (Figure 7), which was the year with the shallowest mean euphotic zone depth (Figure 5). When considering the role light availability has on submerged aquatic vegetation health, a decrease in seagrass health and subsequently habitat area is congruent with a shallower euphotic zone (Ralph et al., 2007).

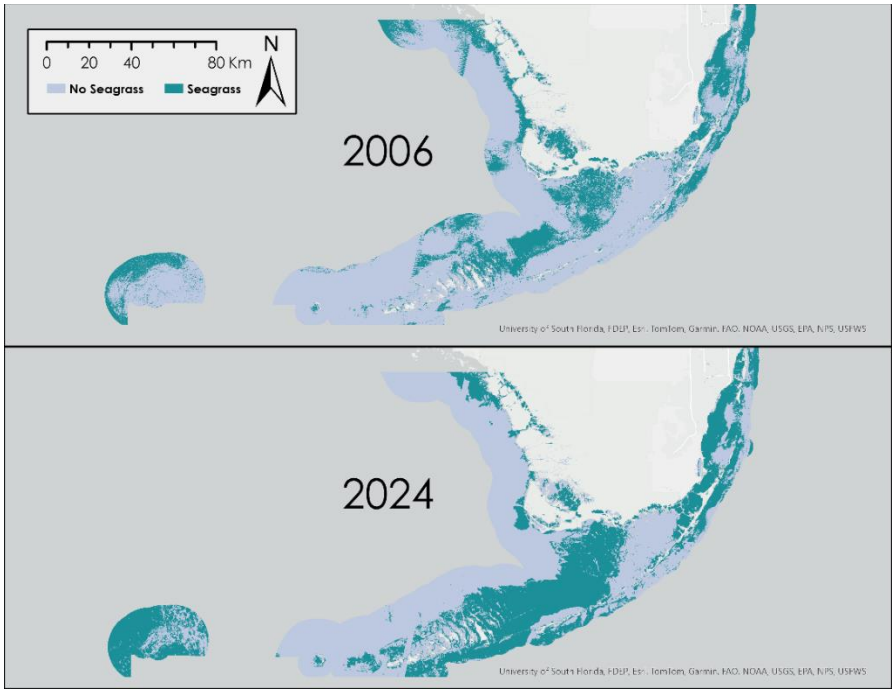

Figure 7. Seagrass Classification Model Outputs for 2006 (top) and 2024 (bottom). Pixels classified as greater than or equal to 5% cover of seagrass are a darker shade of blue, and pixels less than 5% are a lighter shade of blue.

4.2 Feasibility & Partner Implementation

4.2.1 Water Quality Analysis Feasibility & Partner Implementation

We found it feasible to analyze water quality parameters within tarpon management zones using both Level-2 and Level-4 data. Using the methods in this study, it would be less time consuming to study every grid cell within the management regions using Landsat Level-2 data, though this would require more interpretation and have lower total coverage. It would require less interpretation and allow more total coverage to use Level-4 products to do the same, but it would result in lower spatial resolution and be more time consuming with high levels of grid cells of interest.

4.2.2 Habitat Mapping Feasibility & Partner Implementation

We found that Landsat imagery could be used to map mangrove habitat extent using a random forest model, although due to time and training data limitations, model performance was constrained (see 3.2.2). To improve the classification model, partners could incorporate additional features such as texture, build region-specific classification models instead of using a single classification model for the entire study area, or use training data that distinguishes healthy versus damaged mangroves.

Regarding seagrass habitat classification, we found that the methodology used with Landsat imagery over a large study area was not feasible. With the combination of training data incompatible with random forest classification modelling, coarse spatial resolution, and time constraints, our seagrass habitat maps could not be determined as an accurate representation of the ecosystem. Like mangrove habitat classification, we

recommend region-specific seagrass classification models as well as the addition of class values that indicate habitat condition. Additionally, as supported by similar studies (Lizcano-Sandoval et al., 2022), we recommend using earth observations with finer resolutions, such as Sentinel, when mapping seagrass habitats.

4.2.3 Feasibility & Partner Implementation Next Term

BTT and FWC will be partnering with a new DEVELOP team during the 2025 summer term, continuing investigations of southern Florida water quality and habitat extents in the Everglades region. This team will use our time series analyses as well as habitat extent maps to inform their own investigation into sediment plume and harmful algal bloom events. Additionally, the future team will develop forecasting models of these phenomena. A goal that our team initially had, but proved to be infeasible within 10 weeks, was comparing our end products findings to Atlantic tarpon tracking data provided by BTT. This data will be provided to the next team in hopes that this information can be used for further comparison and analysis.

5. Acknowledgements

Partners and Collaborators:

- **Dr. Kara Radabaugh**, **Becca Hatchell**, **Dr. Brad Furman** – Florida Fish and Wildlife Conservation Commission, Fish and Wildlife Research Institute
- **Dr. Aaron Adams**, **Dr. Steven Lombardo, Dr. Lucas Griffin** – Bonefish & Tarpon Trust

Advisors:

- **Dr. Morgan Gilmour, Dr. Juan Torres-Pérez** – NASA Ames Research Center

NASA DEVELOP Leads and Fellow:

- **Lauren Webster**, **Katie Miller**, **Maya Hall** – Analytical Mechanics Associates

This material contains modified Copernicus Sentinel data (2002-2024), processed by ESA.

Any opinions, findings, and conclusions or recommendations expressed in this material are those of the author(s) and do not necessarily reflect the views of the National Aeronautics and Space Administration.

This material is based upon work supported by NASA through contract 80LARC23FA024.

6. Glossary

ArcGIS – Geographic Information System software provided by Esri
AMSR-E – Advanced Microwave Scanning Radiometer-EOS
API – Application Programming Interface
AVHRR – Advanced Very High Resolution Radiometers
BTT – The Bonefish & Tarpon Trust
CHIIMP – Coastal Habitat Integrated Mapping and Monitoring Programs
Chl-*a* – Chlorophyll-*a,* a form of chlorophyll used in oxygenic photosynthesis
DMSP – Defense Meteorological Satellite Program
Earth observations – Satellites and sensors that collect information about the Earth's physical, chemical, and biological systems over space and time
Envisat – "Environmental Satellite", Part of the ESA's fleet of earth observing satellites
ESA – European Space Agency
ETM+ – Enhanced Thematic Mapper Plus
EUMETSAT – The European Organization for the Exploitation of Meteorological Satellites
FWC – Florida Fish and Wildlife Conservation Commission
FWC–FWRI – Florida Fish and Wildlife Conservation Commission - Fish and Wildlife Research Institute
IUCN – International Union for Conservation of Nature
JAXA – Japan Aerospace Exploration Agency
Kd_490 – Downwelling attenuation coefficient at 490 nm, indicates how strongly light attenuates in a water column for the wavelength 490 nm
Landsat – A NASA/USGS satellite program
MERIS – Medium Resolution Imaging Spectrometer
MNDWI – Modified Normalized Difference Water Index
MODIS – Moderate Resolution Imaging Spectroradiometer
MUR SST – Multi-Scale Ultra High-Resolution SST Analysis
NASA – National Aeronautics and Space Administration
NDAVI – Normalized Difference Aquatic Vegetation Index
NDCI – Normalized Difference Chlorophyll Index
NDMI – Normalized Difference Moisture Index
NDTI – Normalized Difference Turbidity Index
NDVI – Normalized Difference Vegetation Index
NDWI – Normalized Difference Water Index
NetCDF – A multidimensional file format

NIR – Near infrared
NOAA – National Oceanic and Atmospheric Administration
OC-CCI – Ocean Colour Climate Change Initiative
OLCI – Ocean and Land Colour Instrument
OLI – Operational Land Imager, sensor aboard Landsat 8
OLI-2 – Operational Land Imager, sensor aboard Landsat 9
POES – Polar Operational Environmental Satellites
Program 296 – Florida Keys National Marine Sanctuary Seagrass Monitoring Project
PySTAC – Python library for working with SpatioTemporal Asset Catalogs
Random forest – Machine learning algorithm that uses an ensemble of decision trees, commonly used for classification or regression
Remote Sensing – Process of collecting information about an object without physically contacting it, in this context collecting information with satellites
SEACAR – Florida Statewide Ecosystem Assessment of Coastal and Aquatic Resources
SeaWiFS – OrbView-2's Sea-viewing Wide Field of View Sensor
SpatioTemporal Asset Catalogs – Standardized format to interact with geospatial information, such as remote sensing data
SSM/I – Special Sensor Microwave Imagers
SST – Sea surface temperature
SWIR – Shortwave infrared
Suomi NPP – Suomi National Polar-orbiting Partnership
Time Series – set of data collected or calculated over intervals of time
TM – Thematic Mapper
Turbidity – measure of the cloudiness or haziness of water caused by suspended particles and organic matter that reduce light penetration
USGS – U.S. Geological Survey
VIIRS – Visible Infrared Imaging Radiometer Suite

7. References

Adams, A. J., & Cooke, S. J. (2015). Advancing the science and management of flats fisheries for bonefish, tarpon, and permit. *Environmental Biology of Fishes*, *98*(11), 2123–2131. https://doi.org/10.1007/s10641015-0446-9

Adams, A. J., Horodysky, A. Z., McBride, R. S., Guindon, K., Shenker, J., MacDonald, T. C., Harwell, H. D., Ward, R., & Carpenter, K. (2014). Global conservation status and research needs for tarpons (Megalopidae), ladyfishes (Elopidae) and bonefishes (Albulidae). *Fish and Fisheries*, *15*(2), 280–311. https://doi.org/10.1111/faf.12017

Adams, A. J., & Murchie, K. J. (2015). Recreational fisheries as conservation tools for mangrove habitats. *American Fisheries Society Symposium*, *83*, 43–56. https://fisheries.org/doi/9781934874424-ch3/

Bindschadler, R. (2013). Ice cores dynamics of the West Antarctic Ice Sheet. *Encyclopedia of Quaternary Science*, 448-455. https://doi.org/10.1016/b978-0-444-53643-3.00032-7

Browder, J. A., Fourqurean, J., Lirman, D., & Nuttle, W. K. (2013). *Benthic Habitat: Seagrasses* [NOAA Technical Memorandum]. https://www.aoml.noaa.gov/ftp/ocd/fletcher/CPO%20documents/MARES_SEFC_ICEM_20131001_Appendix_Seagrasses.pdf

Bulgin, C.E., Merchant, C.J. & Ferreira, D. (2020) Tendencies, variability and persistence of sea surface temperature anomalies. *Scientific Reports, 10,* 7986. https://doi.org/10.1038/s41598-020-64785-9

Buma, W. G., Lee, S-I. (2020). Evaluation of Sentinel-2 and Landsat 8 images for estimating chlorophyll-a concentrations in Lake Chad, Africa. *Remote Sensing, 12*(15), 2437. https://doi:10.3390/rs12152437

Carlson, D. F., Yarbro, L. A., Scolaro, S., Poniatowski, M., McGee-Absten, V., & Carlson, P. R. (2018). Sea surface temperatures and seagrass mortality in Florida Bay: Spatial and temporal patterns discerned from MODIS and AVHRR data. *Remote Sensing of Environment*, *208*, 171–188. https://doi.org/10.1016/j.rse.2018.02.014

Dogliotti, A. I., Ruddick, K. G., Nechad, B., Doxaran, D., & Knaeps, E. (2015). A single algorithm to retrieve turbidity from remotely-sensed data in all coastal and estuarine waters. *Remote Sensing of Environment, 156*, 157–168. https://doi.org/10.1016/j.rse.2014.09.020

Doyle, T.W., Girod, G.F. (1997). The Frequency and Intensity of Atlantic Hurricanes and Their Influence on the Structure of South Florida Mangrove Communities. In: Diaz, H.F., Pulwarty, R.S. (eds) Hurricanes. Springer, Berlin, Heidelberg. https://doi.org/10.1007/978-3-642-60672-4_6

Earth Resources Observation and Science (EROS) Center. (2020a). Landsat 4-5 Thematic Mapper Level-2, Collection 2 [dataset]. U.S. Geological Survey. https://doi.org/10.5066/P9IAXOVV.

Earth Resources Observation and Science (EROS) Center. (2020b). Landsat 7 Enhanced Thematic Mapper Plus (ETM+) Level-2, Collection 2 [dataset]. U.S. Geological Survey. https://doi.org/10.5066/F7WH2P8G.

Earth Resources Observation and Science (EROS) Center. (2020c). Landsat 8-9 Operational Land Imager / Thermal Infrared Sensor Level-2, Collection 2 [dataset]. U.S. Geological Survey. https://doi.org/10.5066/P9OGBGM6.

Espinoza-Morriberón, D., Aristóteles, M., Jara, H. J., Hervé Demarcq, Larry, J., Alejandro, J., Isaac, P., Aburto, R. M., & Jhon. (2024). Evaluating MODIS sea surface temperature data and chlorophyll-a data from both MODIS and SeaWiFS in the Peruvian Coastal Upwelling System. *Journal of Applied Remote Sensing*, 19(01). https://doi.org/10.1117/1.jrs.19.014505

Fedler, Tony. (2009). *The Economic Impact of Recreational Fishing in the Everglades Region*. The Everglades Foundation. https://www.bonefishtarpontrust.org/downloads/research-reports/stories/everglades-economics-report.pdf

Fedler, Tony. (2011). *The Economic Impact of Recreational Tarpon Fishing in the Caloosahatchee River and Charlotte Harbor Region of Florida*. The Everglades Foundation. https://www.bonefishtarpontrust.org/downloads/research-reports/stories/caloosahatchee-final-economics-report-wexsum.pdf

Florida Fish and Wildlife Conservation Commission (FWC). (2023a). *Mangroves Florida* [dataset]. https://geodata.myfwc.com/datasets/myfwc::mangrove-habitat-in-florida/about

Florida Fish and Wildlife Conservation Commission (FWC). (2023b). *Shoreline Polygon 1:12,000 Scale Florida 2004* [dataset]. https://geodata.myfwc.com/datasets/myfwc::florida-shoreline-1-to-12000-scale/about

Florida Fish and Wildlife Conservation Commission (FWC). (2024). Seagrass Florida [dataset]. https://geodata.myfwc.com/datasets/myfwc::seagrass-habitat-in-florida/about

Florida International University; National Oceanic and Atmospheric Administration (NOAA); National Marine Sanctuaries Program. (2021). Florida Keys National Marine Sanctuary Seagrass Monitoring Project. **(**2022**)**. [dataset]. SEACAR Data Discovery Interface, Office of Resilience and Coastal Protection, Florida Department of Environmental Protection. https://data.florida-seacar.org/programs/details/296

Gao, B. (1996). NDWI—A normalized difference water index for remote sensing of vegetation liquid water from space. *Remote Sensing of Environment*, *58*(3), 257–266. https://doi.org/10.1016/S0034-4257(96)00067-3

Ha, N. T. T., Koike, K., Nhuan, M. T., Canh, B. D., Thao, N. T. P., & Parsons, M. (2017). Landsat 8/OLI two bands ratio algorithm for chlorophyll-a concentration mapping in hypertrophic waters: An application to West Lake in Hanoi (Vietnam). *IEEE Journal of Selected Topics in Applied Earth Observations and Remote Sensing, 10(11)*, 4919–4929. https://doi.org/10.1109/JSTARS.2017.2739184

Hall, M., Furman, B., Merello, M., Durako, M. (2016). Recurrence of *Thalassia testudinum* seagrass die-off in Florida Bay: Initial observations. *Marine Ecology Progress Series, 560*, 243-249. https://doi.org/10.3354/meps11923

Han, X., Feng, L., Hu, C., & Kramer, P. (2018). Hurricane-induced changes in the Everglades National Park mangrove forest: Landsat observations between 1985 and 2017. *Journal of Geophysical Research: Biogeosciences*, *123*(11), 3470–3488. https://doi.org/10.1029/2018JG004501

Jamaluddin, I., Chen, Y.-N., Ridha, S. M., Mahyatar, P., & Ayudyanti, A. G. (2022). Two decades mangroves loss monitoring using random forest and Landsat data in East Luwu, Indonesia (2000–2020). *Geomatics*, *2*(3), Article 3. https://doi.org/10.3390/geomatics2030016

JPL MUR MEaSUREs Project. 2015. GHRSST Level 4 MUR Global Foundation Sea Surface Temperature Analysis. Ver. 4.1. PO.DAAC, CA, USA. Dataset accessed [2025-02-01] at https://doi.org/10.5067/GHGMR-4FJ04

Lagomasino, D., Fatoyinbo, T., Castañeda-Moya, E., Cook, B. D., Montesano, P. M., Neigh, C. S. R., Corp, L. A., Ott, L. E., Chavez, S., & Morton, D. C. (2021). Storm surge and ponding explain mangrove dieback in southwest Florida following Hurricane Irma. *Nature Communications*, *12*(1), 4003. https://doi.org/10.1038/s41467-021-24253-y

Lee, Z.-P. (2005). A model for the diffuse attenuation coefficient of downwelling irradiance. *Journal of Geophysical Research*, 110(C2). https://doi.org/10.1029/2004jc002275

Li, Y., Bai, J., Chen, S., Chen, B., & Zhang, L. (2023). Mapping seagrasses on the basis of Sentinel-2 images under tidal change. *Marine Environmental Research*, *185*, 105880. https://doi.org/10.1016/j.marenvres.2023.105880

Liang, H., Wang, L., Wang, S., Sun, D., Li, J., Xu, Y., & Zhang, H. (2023). Remote sensing detection of seagrass distribution in a marine lagoon (Swan lake), China. *Optics Express*, *31*(17), 27677. https://doi.org/10.1364/OE.498901

Lizcano-Sandoval, L., Anastasiou, C., Montes, E., Raulerson, G., Sherwood, E., & Muller-Karger, F. E. (2022). Seagrass distribution, areal cover, and changes (1990–2021) in coastal waters off West-Central Florida, USA. *Estuarine, Coastal and Shelf Science*, *279*, 108134. https://doi.org/10.1016/j.ecss.2022.108134

Lombardo, S., Black, B., Boucek, R., Adams, A. (2024). Assessing Historical Shifts in the Data Limited Lower Keys Tarpon Fishery, Bonefish & Tarpon Trust. https://www.bonefishtarpontrust.org/wp-content/uploads/2024/07/Lower-Keys-Tarpon-Fishery-Assessment-Final.pdf

McFeeters, S. K. (1996). The use of the Normalized Difference Water Index (NDWI) in the delineation of open water features. *International Journal of Remote Sensing*, *17*(7), 1425–1432. https://doi.org/10.1080/01431169608948714

Mishra, S., & Mishra, D. R. (2012) Normalized difference chlorophyll index: A novel model for remote estimation of chlorophyll-a concentration in turbid productive waters. *Remote Sensing of Environment, 117*, 394-406. https://doi:10.1016/j.rse.2011.10.016.

Ralph, P. J., Durako, M. J., Enríquez, S., Collier, C. J., & Doblin, M. A. (2007). Impact of light limitation on seagrasses. *Journal of Experimental Marine Biology and Ecology*, *350*(1), 176–193. https://doi.org/10.1016/j.jembe.2007.06.017

Rhyma, P.P., Norizah, K., Ismail, A. A. M., & Shamsudin, I. (2016). A review of uses of satellite imagery in monitoring mangrove forests. *IOP Conference Series: Earth and Environmental Science*, *37*(1), 012034. https://doi.org/10.1088/1755-1315/37/1/012034

Rouse, J. W., Haas, R. H., Deering, D. W., & Schell, J. A. (1973). *Monitoring the vernal advancement and retrogradation (green wave effect) of natural vegetation* (RSC-1978-2). https://ntrs.nasa.gov/citations/19740004927

Samper-Villarreal, J., Lovelock, C. E., Saunders, M. I., Roelfsema, C., Mumby, P. J. (2016). Organic carbon in seagrass sediments is influenced by seagrass canopy complexity, turbidity, wave height, and water depth. *Limnology and Oceanography*. *61*(3), 938-952, https://doi.org/10.1002/lno.10262

Sathyendranath, S., Jackson, T., Brockmann, C., Brotas, V., Calton, B., Chuprin, A., Clements, O., Cipollini, P., Danne, O., Dingle, J. , Donlon, C., Grant, M., Groom, S., Krasemann, H., Lavender, S., Mazeran, C., Mélin, F., Müller, D. , Steinmetz, F., Valente, A., Zühlke, M., Feldman, G., Franz, B., Frouin, R., Werdell, J., & Platt, T. (2023): ESA Ocean Colour Climate Change Initiative (Ocean_Colour_cci): Monthly climatology of global ocean colour data products at 4km resolution, Version 6.0. NERC EDS Centre for Environmental Data Analysis, *March 12, 2025*. https://catalogue.ceda.ac.uk/uuid/690fdf8f229c4d04a2aa68de67beb733/

Topouzelis, K., Makri, D., Stoupas, N., Papakonstantinou, A., & Katsanevakis, S. (2018). Seagrass mapping in Greek territorial waters using Landsat-8 satellite images. *International Journal of Applied Earth Observation and Geoinformation*, *67*, 98–113. https://doi.org/10.1016/j.jag.2017.12.013

Tran, T. V., Reef, R., & Zhu, X. (2022). A Review of Spectral Indices for Mangrove Remote Sensing. *Remote Sensing*, *14*(19), 4868. https://doi.org/10.3390/rs14194868

United States Geological Survey. (n.d.). *How do I use a scale factor with Landsat Level-2 science products?* https://www.usgs.gov/faqs/how-do-i-use-a-scale-factor-landsat-level-2-science-products

Villa, P., Laini, A., Bresciani, M., & Bolpagni, R. (2013). A remote sensing approach to monitor the conservation status of lacustrine *Phragmites australis* beds. *Wetlands Ecology and Management*, *21*(6), 399–416. https://doi.org/10.1007/s11273-013-9311-9

Villa, P., Mousivand, A., & Bresciani, M. (2014). Aquatic vegetation indices assessment through radiative transfer modeling and linear mixture simulation. *International Journal of Applied Earth Observation and Geoinformation*, *30*, 113–127. https://doi.org/10.1016/j.jag.2014.01.017

Wabnitz, C. C., Andréfouët, S., Torres-Pulliza, D., Müller-Karger, F. E., & Kramer, P. A. (2008). Regional-scale seagrass habitat mapping in the Wider Caribbean region using Landsat sensors: Applications to conservation and ecology. *Remote Sensing of Environment*, *112*(8), 3455–3467. https://doi.org/10.1016/j.rse.2008.01.020

Wilson, E. H., & Sader, S. A. (2002). Detection of forest harvest type using multiple dates of Landsat TM imagery. *Remote Sensing of Environment*, *80*(3), 385–396. https://doi.org/10.1016/S0034-4257(01)00318-2

Xu, H. (2006). Modification of normalised difference water index (NDWI) to enhance open water features in remotely sensed imagery. *International Journal of Remote Sensing*, *27*(14), 3025–3033. https://doi.org/10.1080/01431160600589179

Zhang, K., Thapa, B., Ross, M., & Gann, D. (2016). Remote sensing of seasonal changes and disturbances in mangrove forest: A case study from South Florida. *Ecosphere*, *7*(6), e01366. https://doi.org/10.1002/ecs2.1366

Zhao, J., Barnes, B., Melo, N., English, D., Lapointe, B., Muller-Karger, F., Schaeffer, B., & Hu, C. (2013). Assessment of satellite-derived diffuse attenuation coefficients and euphotic depths in South Florida Coastal Waters. *Remote Sensing of Environment*, *131*, 38–50. https://doi.org/10.1016/j.rse.2012.12.009

8. Appendices

Appendix A: *Additional mangrove classification figures and tables*

Table A1. *Relative feature importance for mangrove classification random forest model.*

Feature	***Relative Importance***
blue	0.08
green	0.02
red	0.04
NIR	0.10
SWIR1	0.07
SWIR2	0.08
MNDWI	0.09
NDMI	0.07
NDVI	0.14
distance to coastline	0.31

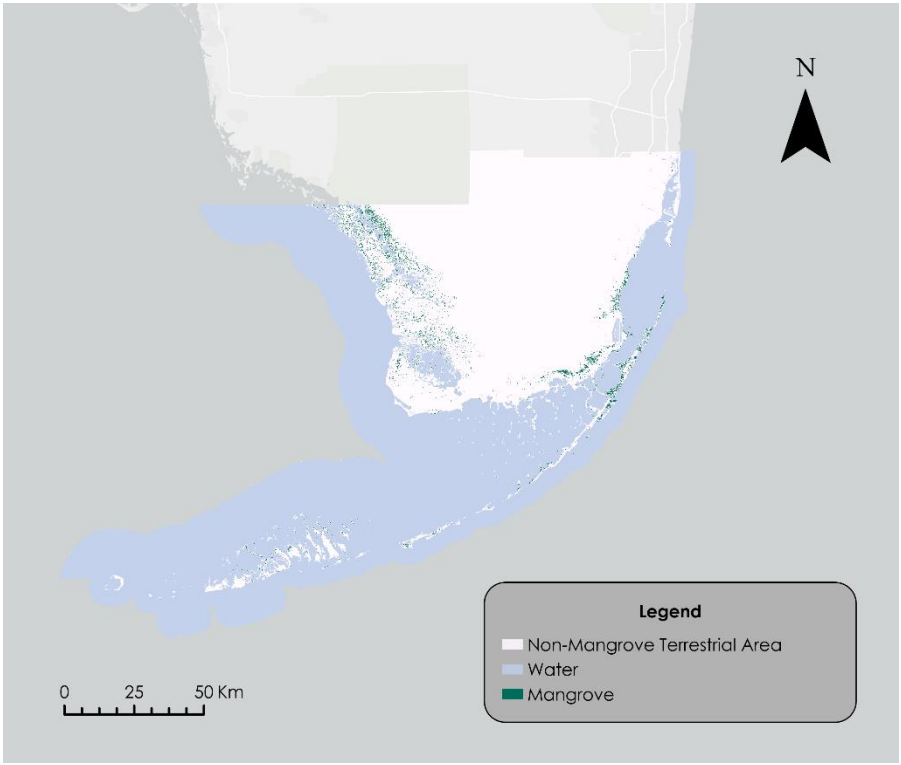

Figure A1. Map of model-classified mangrove habitat for 2006.

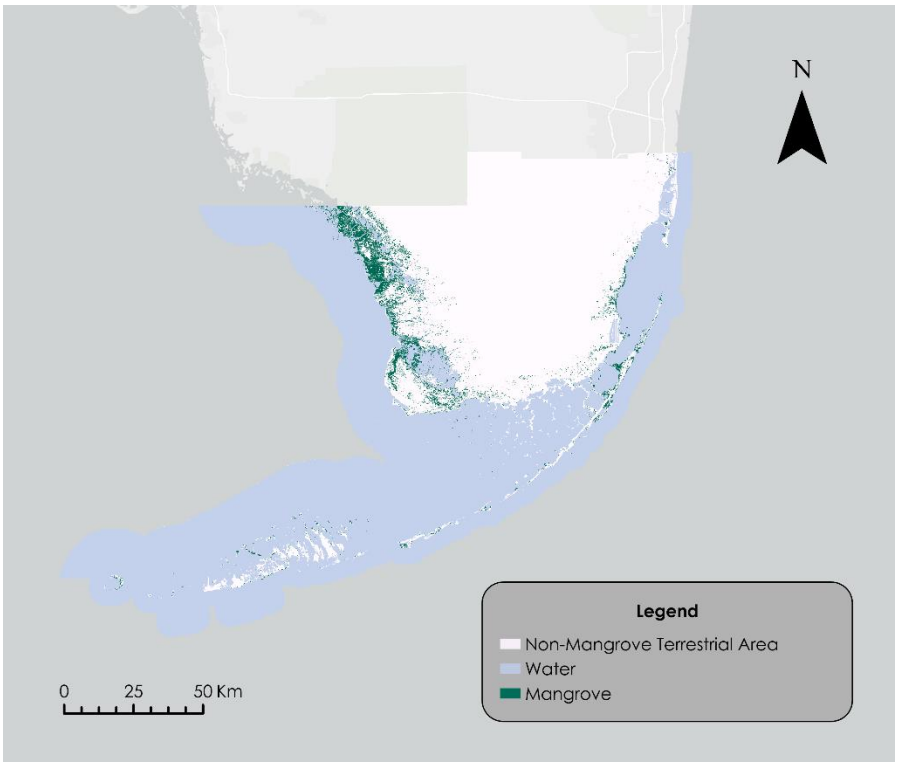

Figure A2. Map of model-classified mangrove habitat for 2010.

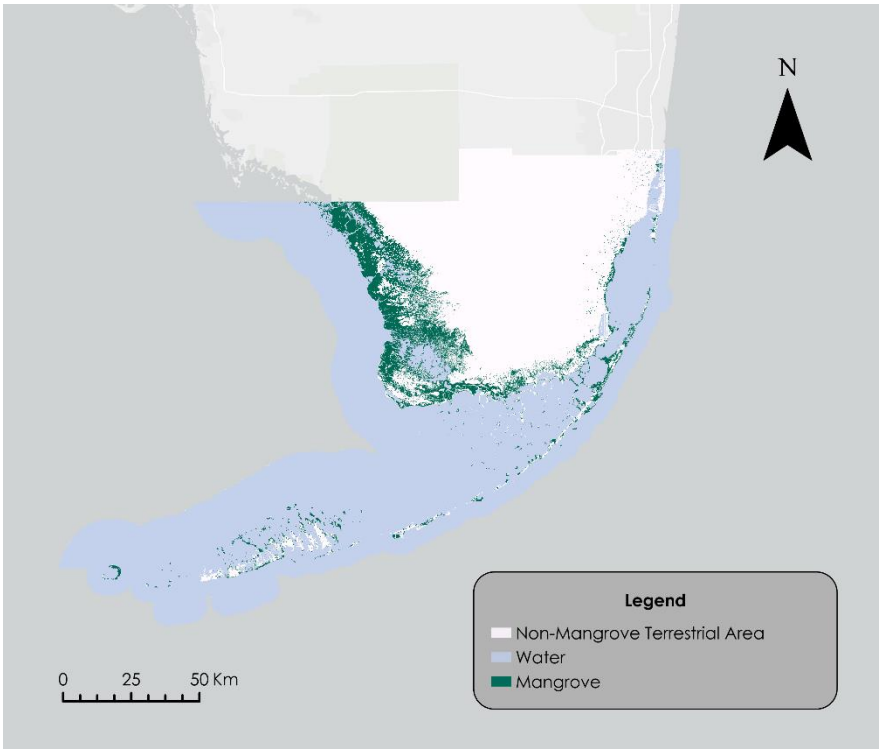

Figure A3. Map of model-classified mangrove habitat for 2015.

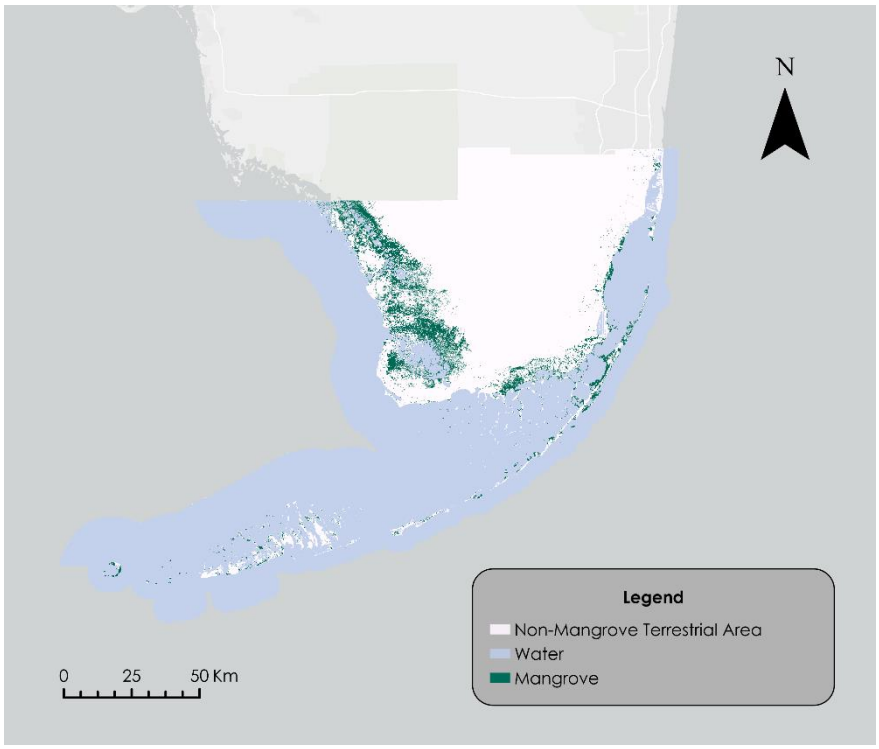

Figure A4. Map of model-classified mangrove habitat for 2018.

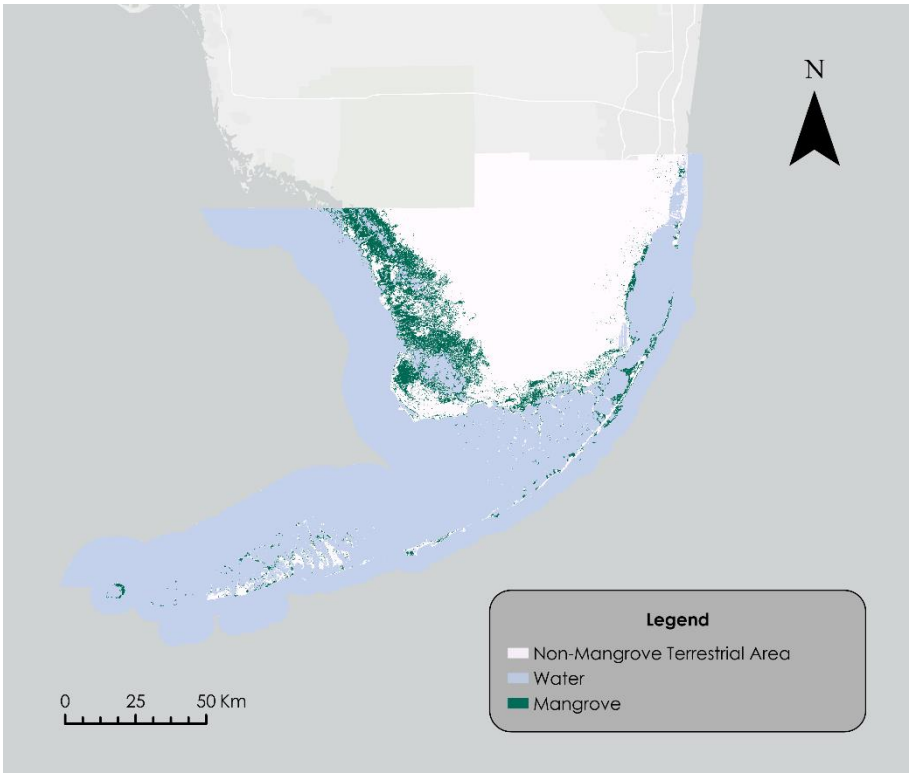

Figure A5. Map of model-classified mangrove habitat for 2019.

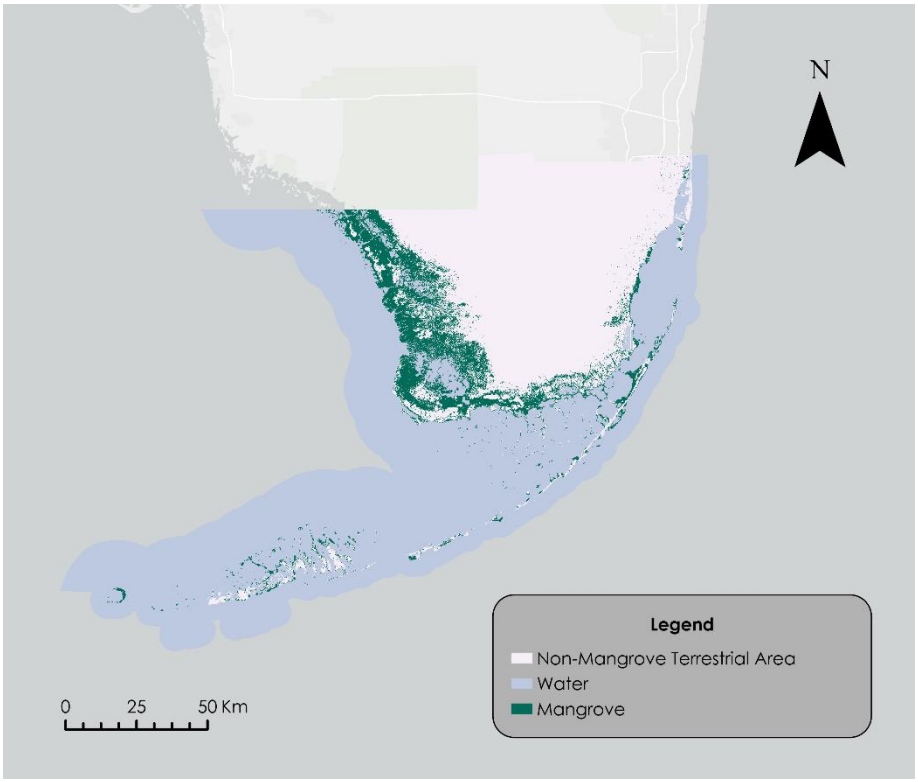

Figure A6. Map of model-classified mangrove habitat for 2024

Appendix B: *Seagrass Habitat Classification Model Metrics and Outputs*

Class Value	Not Seagrass	Seagrass
Not Seagrass	125	42
Seagrass	220	104
	Kappa = 5%	

Figure B1. Confusion Matrix for Pixel-Based Random Forest model

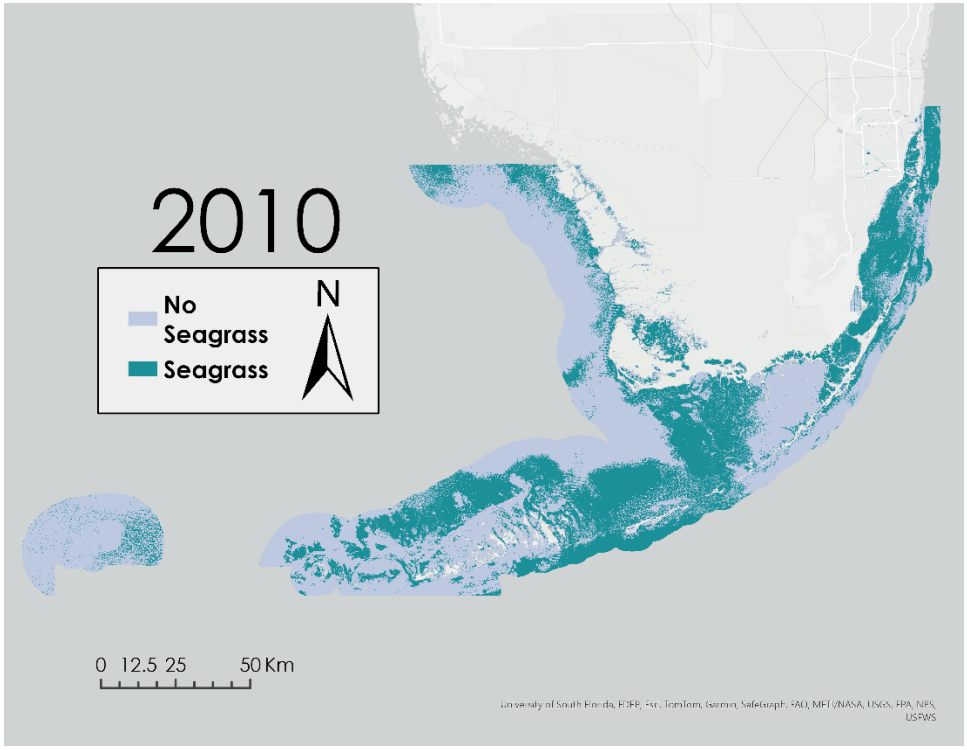

Figure B2. Map of model-classified seagrass habitat for 2010.

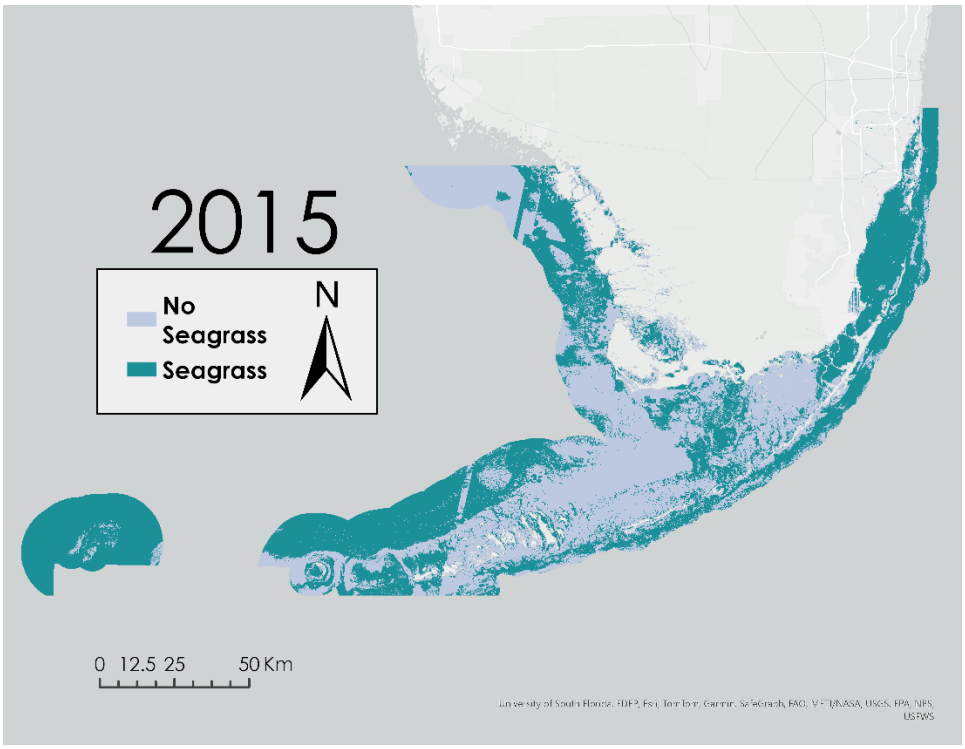

Figure B3. Map of model-classified seagrass habitat for 2015.

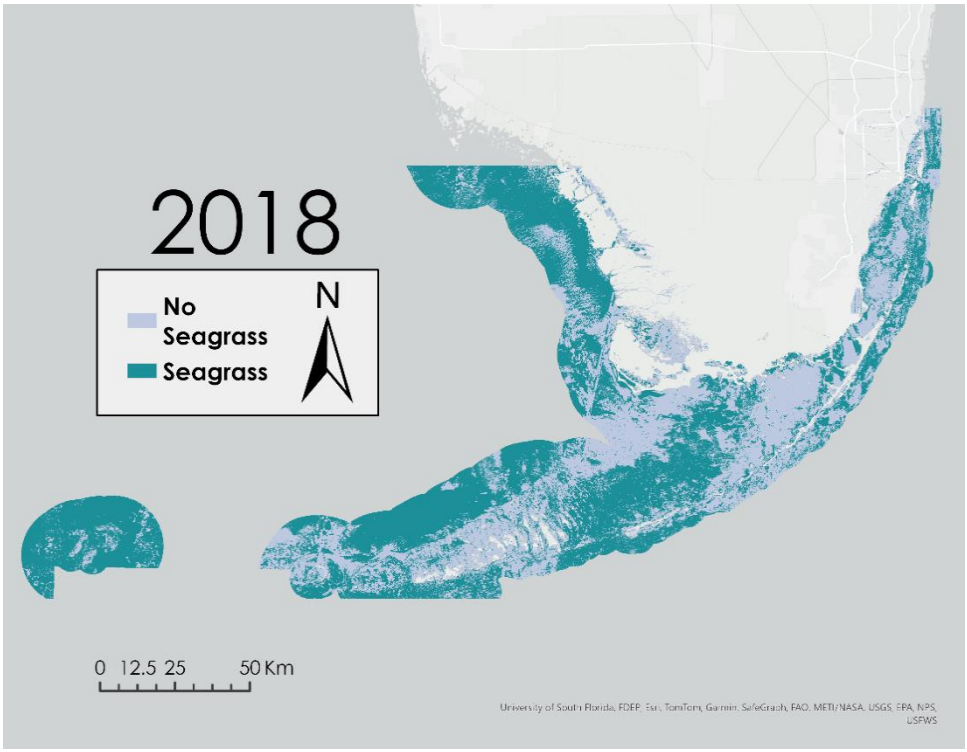

Figure B4. Map of model-classified seagrass habitat for 2018.

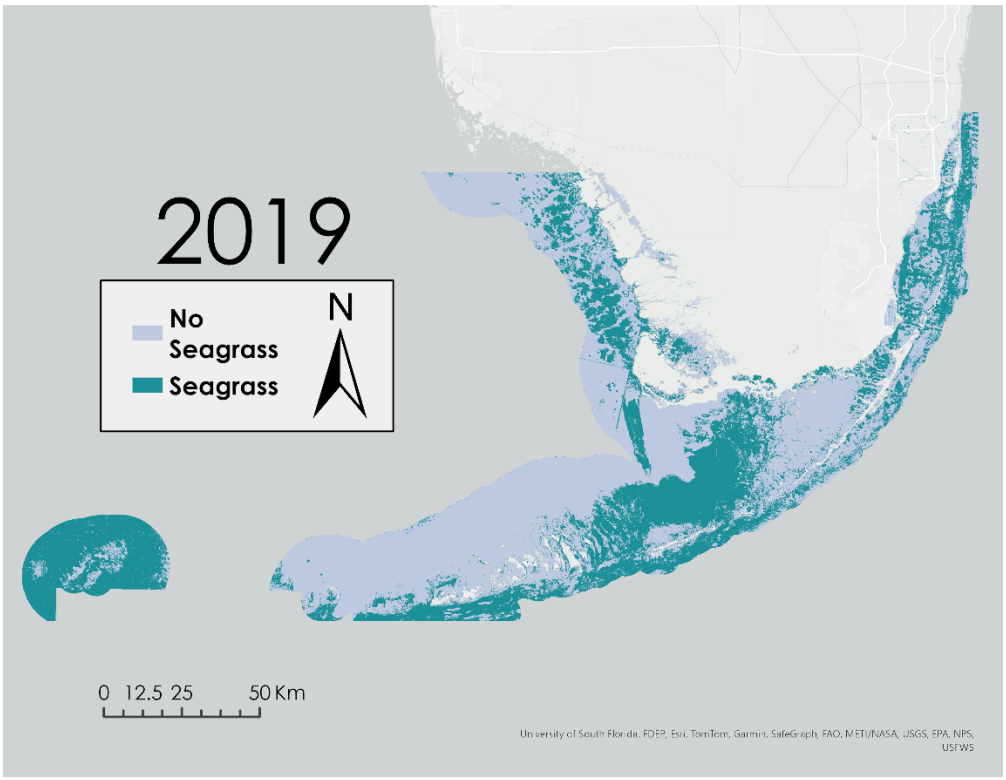

Figure B5. Map of model-classified seagrass habitat for 2019.

Appendix C: *Additional NDTI and NDCI Plots*

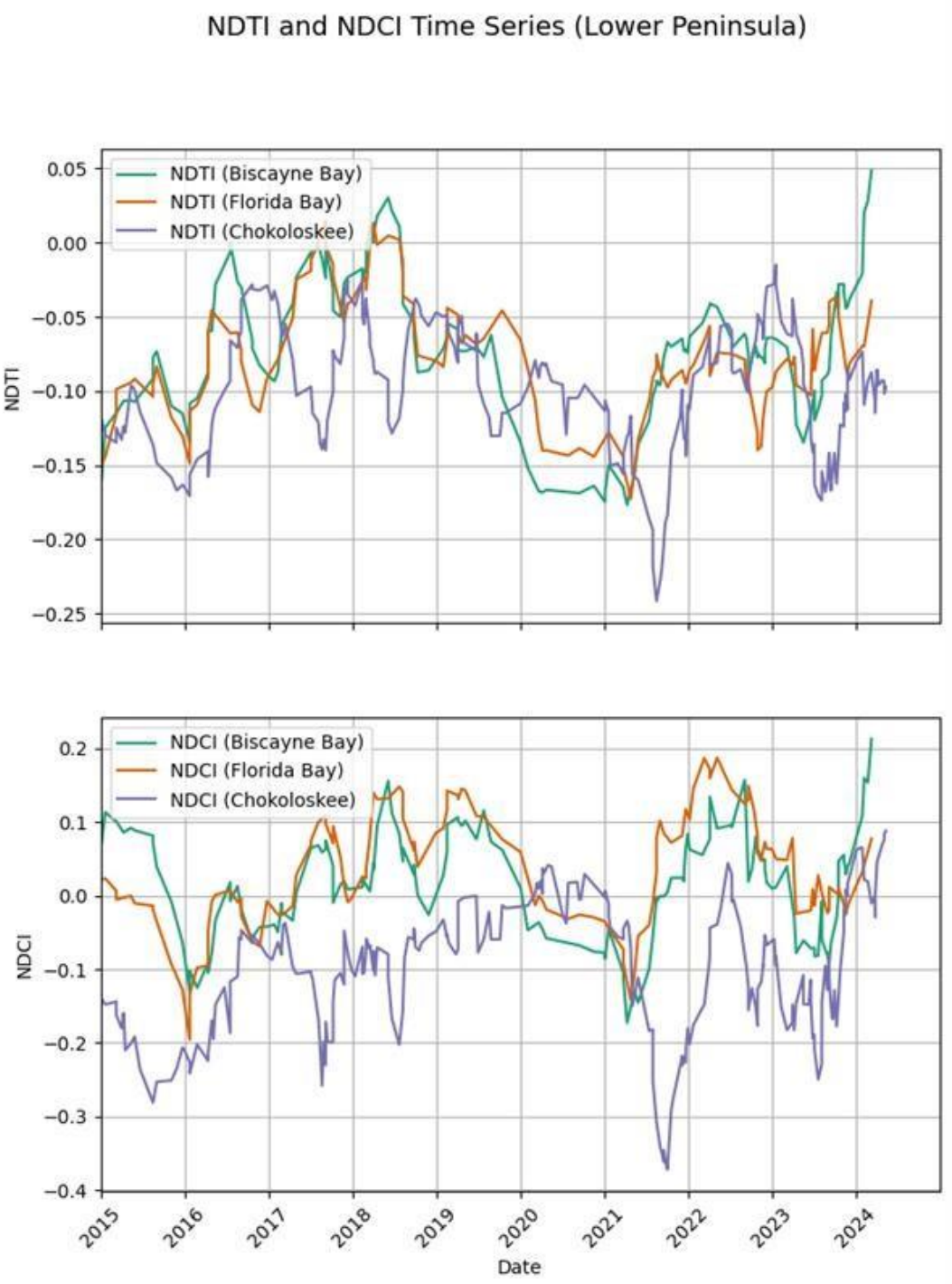

Figure C1. Time Series Plots of NDTI and NDCI for Biscayne Bay, Florida Bay, and Chokoloskee

Appendix D: *Linear Regression of Minimum SST in Tarpon Management Regions*

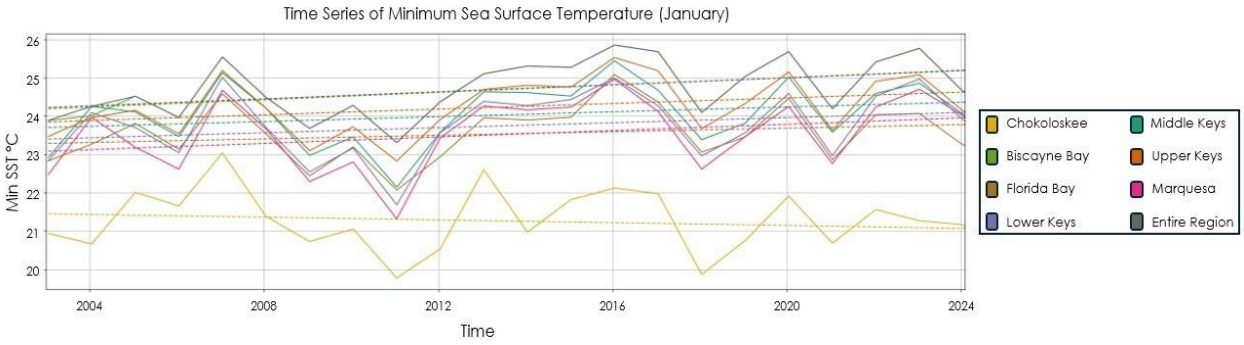

Figure D1: The minimum pixel value of SST from each management area during January, plotted from 2003 - 2024. The dashed trendlines are the same color as the solid lines, each representing one of seven management regions. The grey dashed line representing all the regions combined.